TOKYO INSTITUTE OF TECHNOLOGY HEAVY-ION LINEAR ACCELERATOR SYSTEM

E. Arai, T. Hattori and Y. Oguri
Nuclear Reactor Research Laboratory, Tokyo Institute of Technology
Ohokayama 2-12, 152 Tokyo-Meguroku

M. Ogawa
Faculty of Energy Sciences, Tokyo Institute of Technology
Nagatsuda 4259, 227 Yokohama-Midoriku

ABSTRACT

Tokyo Institute of Technology started a heavy-ion lineac project for fusion-reactor research and for heavy-ion atomic and nuclear physics. The system is accomplished in 1984 up to the second lineac. The lineac structure and its experimental as well as theoretical design studies are described. An optimum design condition has been determined.

SPECIFICATION OF THE TOKYO INSTITUTE OF TECHNOLOGY LINEAC SYSTEM

Figure 1 shows the layout of the system which consists of one injector and two lineacs. The injector is an NEC 5SDH-HC2 tandem with a maximum terminal voltage of 1.6 MV. A sputter type and a PIG type ion sources are connected to the tandem through a switching magnet. A gas stripper is equipped for the charge exchange in the high-voltage terminal.

This economical tandem is able to accelerate ions up to $\beta=2\%$ in the mass number range of 12 to 50. This β value has two advantages : 1) We can design drift tubes with focusing elements adopting π-π mode. 2) For the ions ranging from lithium to chlorine, the fraction of the ions stripped in a carbon foil is not too small at $q/A=1/4$, which is the design value for the lineac.[1]

Figure 2 shows the IH structure of the first lineac. Because of the cooling and wiring of the focusing element in the drift tubes, the beam axis is asymmetrically located in the cavity. The drift tubes without quadrupole magnets are connected to the top of the stems which are mounted on a ridge. The drift tubes with a quadrupole magnet are mounted on the top of the stems which are suspended from the cavity wall through diaphragms.

Characteristic are two pairs of wings in the low-energy section and a magnetic flux inducer at the high-energy end. The wings form a short circuit between the top of the ridge and two lines on the inner surface of the resonator tank. The tank inductance is reduced at the low-energy section to compensate the local eigenfrequency decrease.[2] We use two pairs of wings in order to temper the effect from the abrupt change of the tank inductance in comparison with the case where only one pair of long wings are used. Two more accelerating gaps are seen on the magnetic flux inducer. Under these electrodes more magnetic flux links the RF circuit in this section in comparison with other sections so that the accelerating voltage is enhanced at the high-energy end of the resonator cavity.

Figure 3 shows the low energy side of the first cavity. The tank was made of copper-clad SS41 steel. The drift tubes suspended from the tank wall include magnetic quadrupole half lenses which are cooled with liquid freon. The outer diameter of the drift tubes is 100 mm. The drift tubes without half lenses are cooled with pure water and have a diameter of 50 mm.

Figure 4 shows the IH structure of the second lineac. The resonance frequency is two times of that of the first cavity and is 97 MHz. We have chosen the structure proposed by the München group[3,4]. The drift tubes include no focusing elements in them. The only difference is that the two drift tubes from both end plates include quadrupole magnets.

Table 1 lists the main features of these two accelerating cavities.

Figure 5 shows the inner structure of the quadru-

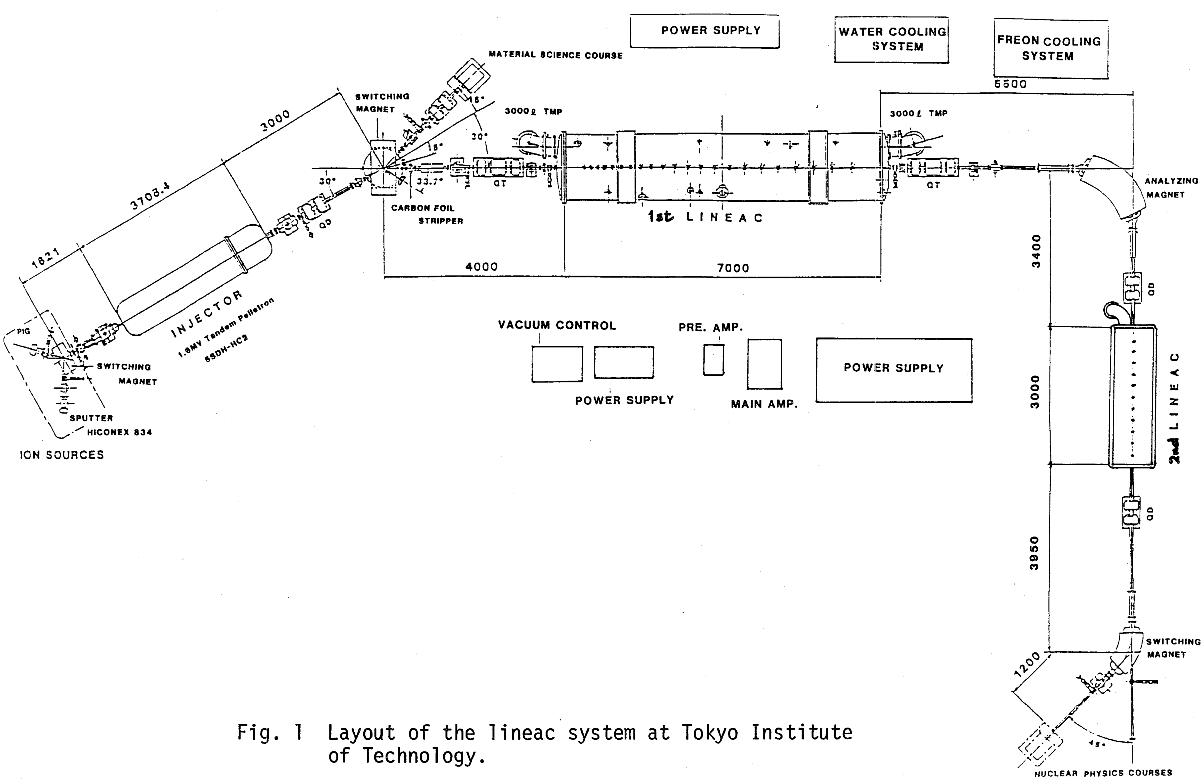

Fig. 1 Layout of the lineac system at Tokyo Institute of Technology.

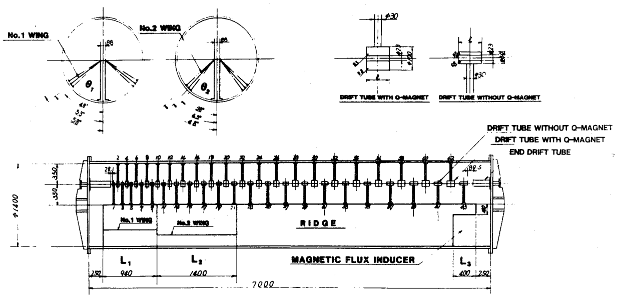

Fig. 2 The Structure of the first lineac cavity.

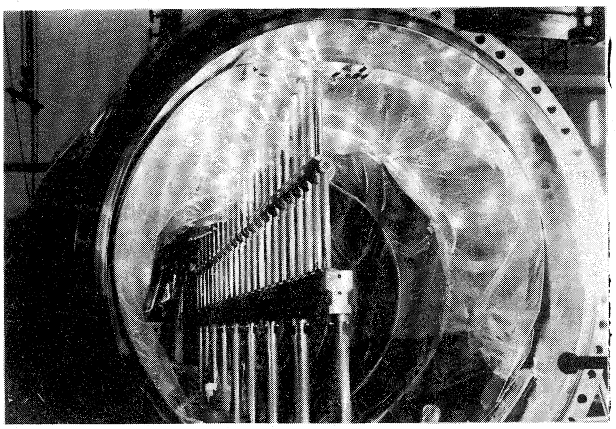

Fig.3 The first lineac cavity photographed from the low energy end.

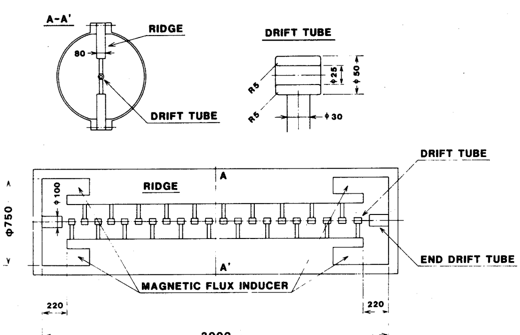

Fig.4 The IH structure of the second accelerating cavity.

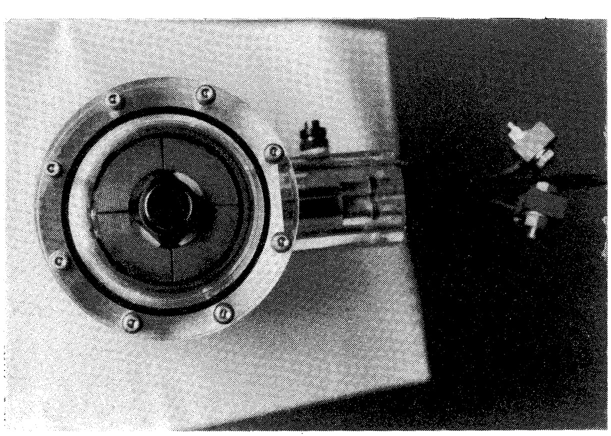

Fig.5 A prototype of quadrupole magnet half lenses equipped in the drift tubes.

pole magnet half lenses. Using spiral plate coils we have observed very stable operation up to a field gradient of 4 kGauss/cm.

Table 1: The main feature of the lineac system

	1st Lineac	2nd Lineac
Injection Energy	0.24 MeV/u	2.5 MeV/u
Output Energy	2.5 MeV/u	3.5 MeV/u
Number of Cells	44	22
Accelerating Frequency	49 MHz	98 MHz
RF Input Power	100 kW max.	50 kW max.
Accelerating Phase	-30°	0°
Species of Ions	All possible ions between Li and Cℓ	All possible ions between Li and Cℓ
Beam Current	1 μA electric	0.5 μA electric
Longitudinal Acceptance	90°	100%
Radial Acceptance	70π mm·mrad	50π mm·mrad
Mode of operation	CW	CW
Length of the RF cavity	7 m	3 m
Inner diameter of the RF cavity	1.4 m	0.75 m
Vacuum system	2 x 3000 $\ell \cdot s^{-1}$ turbo-molecular pumps	1 x 1500 $\ell \cdot s^{-1}$ turbo-molecular pump

In the following sections we describe results of experimental and theoretical works for optimization of distribution of the accelerating field in the first cavity.

RESULTS OF SCALE MODEL EXPERIMENTS FOR THE FIRST ACCELERATING CAVITY

Brass scale models were constructed to measure fundamental parameters for the design work. The field distributions were measured by means of the perturbation technique. An equivalent circuit analysis was also performed in parallel with the experimental study.

Equivalent circuit analysis of field distributions

Figure 6-a shows an equivalent circuit for each cell. The ohmic resistance was neglected. The parallel inductance L_t was calculated from the diameter of the cavity. The stem inductance L_s was determined from the length and the diameter of the stems. The capacity C was measured for each drift tube. The series inductance L_ℓ corresponds to the longitudinal component of the surface current in the cavity, and has been extracted from the dispersion relation given as follows:

$$\beta^2 = \omega^2 L_\ell \left(\frac{C}{1 - \omega^2 L_s C} - \frac{1}{\omega^2 L_t} \right)$$

where ω and β denote the resonant angular frequency and phase constant of the wave, respectively.

Using these parameters we express each cell as a matrix. The whole cavity was simulated by the sequential multiplication of the matrixes.

Accelerating field distribution before adjustment

Figure 6-b shows the result of accelerating-field distribution measurements. The cavity has no short-circuit wings and the inducer was closed by brass plates to interrupt the additional RF magnetic flux. A strong concentration of the field is seen in the low-energy region of the cavity. The curve shows the theoretical prediction obtained by the equivalent circuit analysis.

Effect of the magnetic flux inducer

Figure 6-c shows the effect of the magnetic flux inducer. For simplicity, we have at first mounted only one pair of wings. The angles and length of the wings were 70° and 350 mm, respectively, and were kept constant through this experiment. The theoretical curves reproduce the experimental results very well. The parameters L_t and L_ℓ were changed at the 45th and 46th cell to reflect the effect of the flux inducer into the equivalent circuit analysis.

The field strength was enhanced at the high-energy end. This effect increases with the inducer length. We

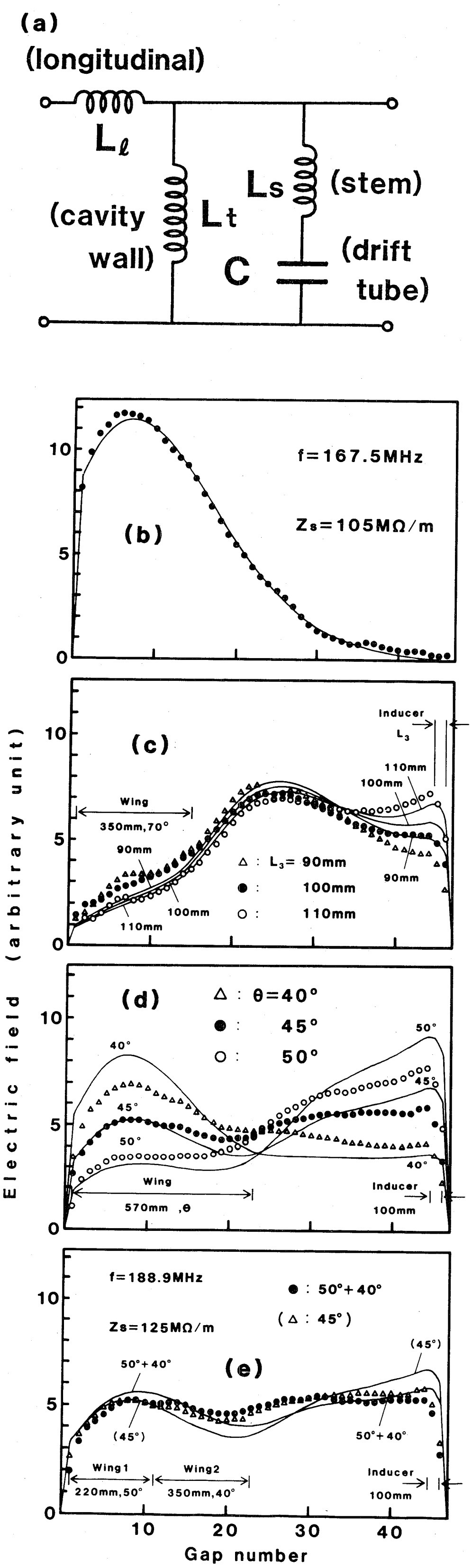

Fig.6 Equivalent circuit for each accelerating cell and variations in the field distribution for various configurations of the tuners. Solid lines are the result of the theoretical calculations.

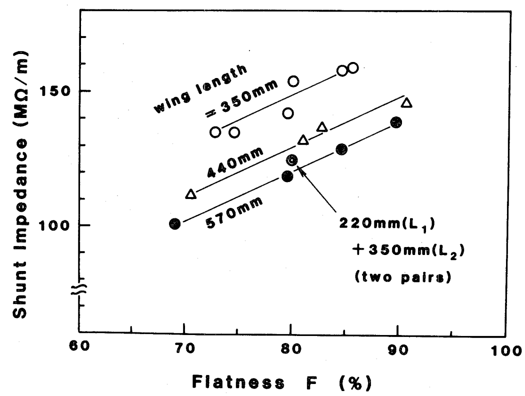

Fig.7 Measured shunt impedances of the model cavity as a function of the flatness F for various wing length.

have chosen 100mm as an optimum length. The optimization of parameters of the short circuit wings was based on this value.

Effect of the short-circuit wing angle

Figure 6-d shows the effect of the wing angle θ on the accelerating field distribution. In this measurement we have had still only one pair of short circuit wings. The field strength in the region of the wings decreases with increase of the wing angle. The curves represent the results of the equivalent circuit analysis. The inductances L_t and L_ℓ in the corresponding region were changed according to the reduction of the cross section.

The field distribution shows a dent at the interface between the region with the wings and that without wings.

In order to avoid the dent, we have introduced one more pair of wings. The result is shown in Fig.6-e. The dent has disappeared and an almost uniform field distribution was obtained.

Influence of the tuners on shunt impedance

In order to investigate the effect of the form of field on the RF power consumption, a shunt impedance of the model cavity was deduced from the perturbation measurements for each tuner configuration. For a quantitative estimations of the shape of the distributions, we defined "flatness" F as follows :

$$F \equiv 1 - \frac{\sigma}{\overline{V}}$$

where $\overline{V}$ and σ denote the mean value and the standard deviation of the gap voltages, respectively. This value was determined for each configuration of the tuners.

The measured shunt impedances are plotted in Fig.7 in terms of the flatness. The result shows that the shunt impedance increases with the flatness F for each wing length. Since the flatness obtainable by this method is limited to at most 90%, the extraporation of the curves to F=100% has no meaning.

REFERENCES

1. E. Arai, T. Hattori, K. Hayashi, M. Ogawa, Y. Oguri and K. Sato, Proc. INS International Symp. Heavy Ion Accelerators and Their Applications to Inertial Fusion (1984)(to be published).
2. N. Ueda, S. Yamada, E. Tojo, T. Hattori, K. Yoshida and T. Hori, IEEE Trans. Nucl. Sci. NS-28, No.3 (1981) 3023.
3. E. Nolte, R. Geier, W. Schollmeier and S. Gustavsson, Nucl. Instr. Meth. 201 (1982) 281.
E. Nolte, G. Geschonke, K. Berdermann, R. Oberschmid, R. Zierl, M. Feil, A. Jahnke, M. Kress and H. Morinaga, Nucl. Instr. Meth. 158 (1979) 311.
4. K. Furuno, T. Kimura and H. Maeoka, Tsukuba University Annual Report, UTTAC-45 (1982) 4.